

Visual Acuity Prediction on Real-Life Patient Data Using a Machine Learning Based Multistage System

Tobias Schlosser^{1,*}, Frederik Beuth¹, Trixy Meyer¹, Arunodhayan Sampath Kumar¹, Gabriel Stolze², Olga Furashova², Katrin Engelmann², and Danny Kowerko¹

¹Junior Professorship of Media Computing, Chemnitz University of Technology, 09107 Chemnitz, Germany

²Department of Ophthalmology, Klinikum Chemnitz gGmbH, 09116 Chemnitz, Germany

*tobias.schlosser@cs.tu-chemnitz.de

ABSTRACT

In ophthalmology, intravitreal operative medication therapy (IVOM) is a widespread treatment for diseases related to the age-related macular degeneration (AMD), the diabetic macular edema (DME), as well as the retinal vein occlusion (RVO). However, in real-world settings, patients often suffer from loss of vision on time scales of years despite therapy, whereas the prediction of the visual acuity (VA) and the earliest possible detection of deterioration under real-life conditions is challenging due to heterogeneous and incomplete data. In this contribution, we present a workflow for the development of a research-compatible data corpus fusing different IT systems of the department of ophthalmology of a German maximum care hospital. The extensive data corpus allows predictive statements of the expected progression of a patient and his or her VA in each of the three diseases. We found out for the disease AMD a significant deterioration of the visual acuity over time. Within our proposed multistage system, we classify the VA progression into the three groups of therapy “winners”, “stabilizers”, and “losers” (WSL scheme). Our OCT biomarker classification using an ensemble of deep neural networks results in a classification accuracy (F1-score) of over 98 %, enabling us to complete incomplete OCT documentations while allowing us to exploit them for a more precise VA modelling process. Our VA prediction requires at least four VA examinations and optionally OCT biomarkers from the same time period to predict the VA progression within a forecasted time frame, whereas our prediction is currently restricted to IVOM / no therapy. While achieving a prediction accuracy of up to 69 % (macro average F1-score) when considering all three WSL-based progression groups, this corresponds to an improvement by 11.2 % in comparison to our ophthalmic expertise (57.8 %).

1 Introduction and motivation

High-resolution imaging of the central retina utilizing optical coherence tomography (OCT) plays a key role in the diagnosis and monitoring of the most common macular diseases such as age-related macular degeneration (AMD), diabetic macular edema (DME), and retinal vein occlusion (RVO)^{1,2}. Furthermore, detailed analysis of different biomarkers on OCT scans is now the basis for treatment decisions as several biological markers provide not only information on diagnosis of these particular eye conditions, but also play an important role in predicting the treatment response. With the increasing amount of available data for therapeutic strategies, the identification of biomarkers with predictive values, as well as different medication options such as intravitreal operative medication therapies (IVOM) for macular edema or diabetic retinopathy patients, it is challenging for ophthalmologists to individualize the therapy for each patient. Artificial intelligence (AI) based algorithms should, in the future, help to find optimal individual therapeutic strategies for each patient. Real-world studies have already demonstrated how important the early treatment begin and the compliance with the therapy are³⁻⁵. The study group of *Gerding et al.* was one of the first ones to classify patients with AMD into three treatment groups based on visual acuity (VA) and central retinal thickness: therapy “winners”, “stabilizers”, and “losers” (WSL scheme)⁶. This interdisciplinary cooperation between IT specialists and ophthalmologists aims at analyzing the patients’ data according to the WSL scheme while identifying predictive values for several OCT biomarkers. The results should help ophthalmologists to better define their therapy strategy for each patient in everyday practice. Moreover, *Schmidt-Erfurth et al.* recently reported the potential of AI-based approaches for targeted optimization of diagnosis and therapy for eye diseases⁷. In their contributions, they furthermore describe the impact of deep learning (DL) for the prediction of patient progressions in the earlier stages of AMD utilizing OCT biomarkers^{8,9}. Whereas current state-of-the-art research also explores the explainability as well as the related nomenclature when reporting AMD-related diseases^{10,11}, AMD as well as DME and RVO can be seen as the three most prevalent investigated eye diseases within the context of AI¹¹⁻¹⁴.

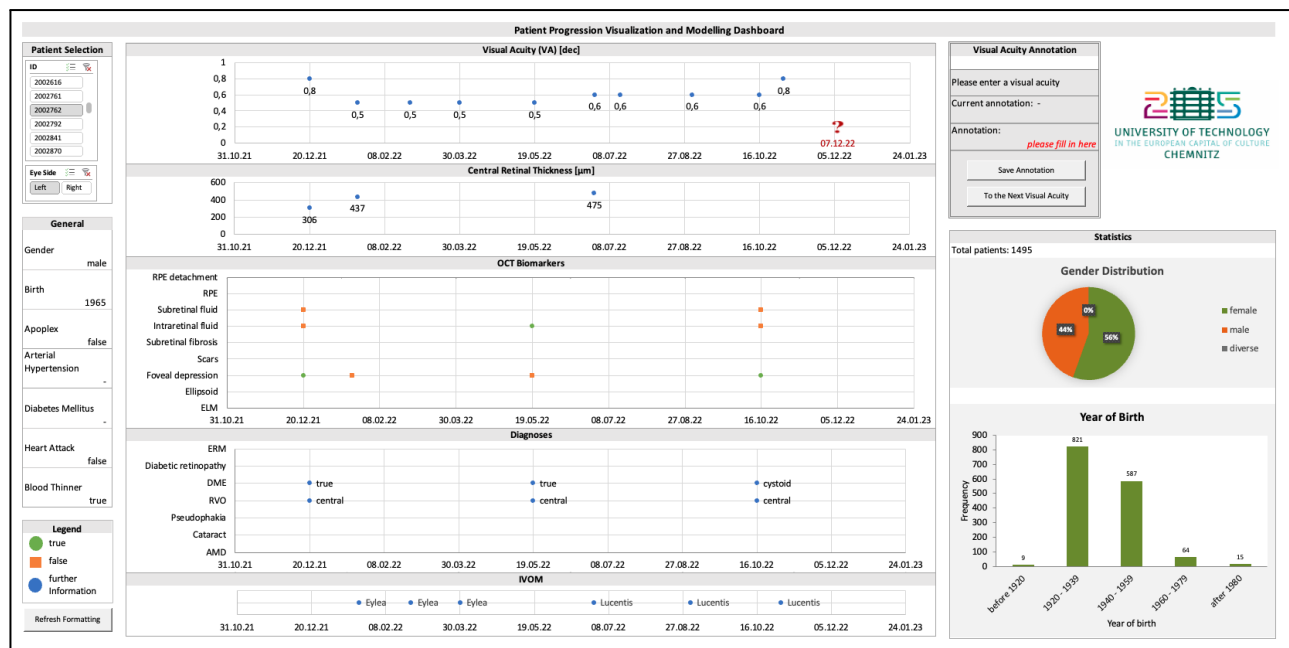


Figure 1. Patient progression visualization and modelling dashboard developed with medical doctors for medical doctors as well as researchers. Visualized are general patient information, VA, OCT biomarkers, diagnoses, and medications. It is possible to annotate the expected course of the VA on site at the position of the red question mark. The shown data set is inspired by real patients and is synthesized to avoid re-identification. The distance between two adjacent vertical guide lines is 50 days.

1.1 Related work

In the following sections, we discuss ophthalmic research on data mining from clinical IT systems (section 1.1.1), text and OCT image processing (section 1.1.2), and the use of the processed data for patient progression modelling (section 1.1.3).

1.1.1 Availability of ophthalmic data in research

In recent years, more and more ophthalmic data sets are being released^{15,16}. A recent review article identified 94 open access data sets containing 507 724 images and 125 videos from 122 364 patients with diabetic retinopathy, glaucoma, and AMD being disproportionately over-represented in comparison to other eye diseases. However, the documentation of demographic characteristics such as age, sex, and ethnicity was reported to be of poor data quality even at the aggregate level¹⁷. In 2017, we proposed a prototypical workflow to aggregate ophthalmic text and image data of all patients from the Department of Ophthalmology of the maximum care hospital Klinikum Chemnitz gGmbH in Chemnitz, Germany. We combined data mining and basic natural language (NLP) processing utilizing the interface of the clinic's practice management software Turbomed (CompuGroup Medical) and extracted a set of preliminary diagnostic patient data in order to determine the ratio of patients with VA improvement, stabilization, and deterioration¹⁸.

1.1.2 Ophthalmic text and OCT image processing

While widely being used for general text processing, NLP systems have recently been demonstrated to robustly extract medication information from clinical notes to study VA, intraocular pressure, and medication outcomes of cataract and glaucoma surgeries^{19,20} to develop predictive models for low-vision prognosis²¹ as well as to predict glaucoma progressions²². Following *De Fauw et al.*, especially machine learning (ML) and deep learning based approaches enable a more precise progression modelling as recent advances prove their applicability and capabilities within the domain²³. Moreover, recognition of OCT biomarkers²⁴ allows further VA and treatment based medical forecasts, including ensemble-based solutions to OCT segmentation²⁵ that enable the completion of incomplete OCT documentations. However, automated thresholding algorithms can yield an improved reproducibility of OCT parameters while allowing a more sensitive diagnosis of pathologies when, e.g., discriminating between healthy and impaired macular perfusion²⁶.

1.1.3 Patient progressing modelling

Schmidt-Erfurth et al. investigate the influence of hyperreflective foci as OCT biomarkers during the progression of geographic atrophy within the context of AMD⁸. While utilizing deep neural networks (DNN) for OCT segmentation²⁷, they identify and localize occurrences given a data set of 87 eyes from 54 different patients. Following *Schmidt-Erfurth et al.*'s contribution,

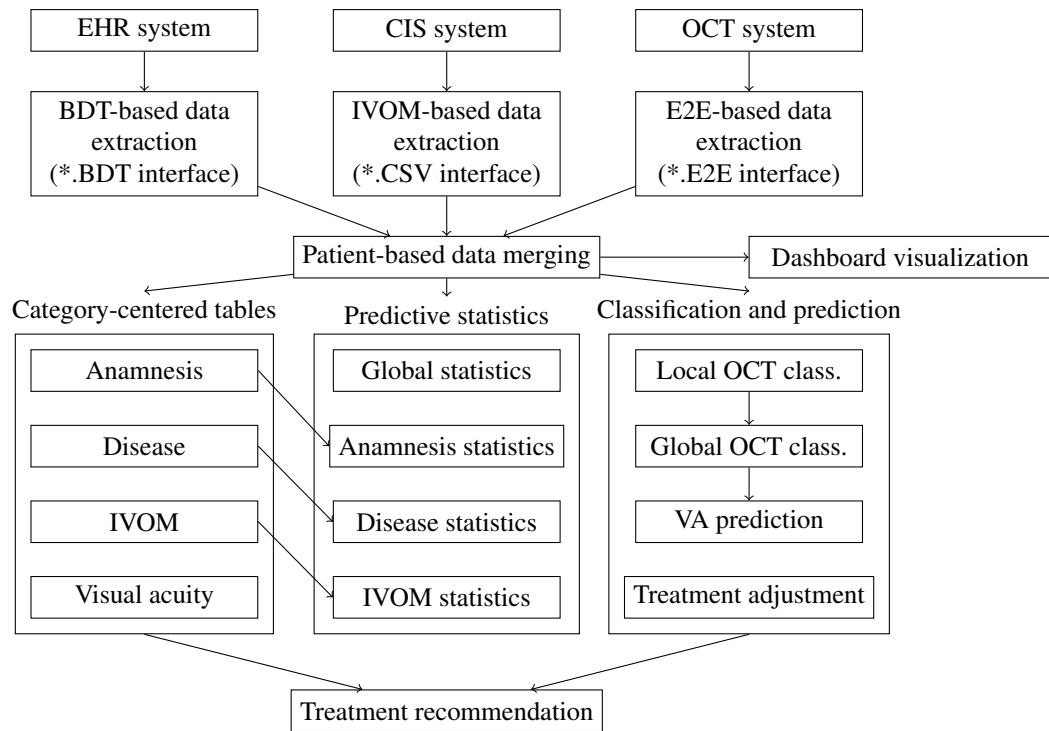


Figure 2. Proposed medical text and image data mining workflow for the following descriptive statistics and VA modelling based on our three base systems of the electronic health record system (EHR or Turbomed system), the clinical information system (CIS system), and the OCT system. Our patient progression visualization and modelling dashboard is shown in Fig. 1. Currently, the classification and prediction step of treatment adjustment is still in development. However, given all data, a treatment recommendation can be realized.

Waldstein *et al.* propose a further developed system while evaluating it with 8 529 OCT volumes of 512 different patients⁹. Moreover, time-dependent sequence modelling using recurrent neural networks (RNN)²⁸ constitutes a promising approach to treatment prediction²⁹. At this point it is also noted that approaches to patient progression modelling exist that explore conventional models. These include mathematical models, e.g., to determine the effect of the anti-vascular endothelial growth factor on VA via medication concentration and tolerance³⁰, as well as regression-based approaches, e.g., to predict VA in diabetic retinopathy via the foveal avascular zone area³¹.

1.2 Contribution of this work

In this contribution, we present an IT system architecture that aggregates patient information for more than 49 000 patients from different categories of various multimedia data in the form of text and images within multiple heterogeneous ophthalmic data resources. The resulting data corpus enables predictive statements to be made about the expected progression of a patient's visual acuity after at least four VA examinations in each of the three diseases – AMD, DME, and RVO. A more fine-grained analysis is conducted to reveal the influence of medical co-existing factors such as other diseases in this real-world setting. Within our proposed multistage system, an ensemble of deep neural networks allows the completion of incomplete or missing OCT documentations. In order to conduct a patient progression modelling, we define a fundamental use case for the prediction of the VA by aggregating different patient information as input of the subsequent VA forecast after a given time period. We present an evaluation formalism and discuss the resulting predictions in comparison to those of a human annotator as our ophthalmic expertise (an experienced ophthalmologist). In order to enable ophthalmic doctors to annotate their predictions regarding the patient-wise expected VA progression, our proposed patient progression visualization and modelling dashboard gives an overview over our aggregated data with patient-wise information of, i.a., general patient information and VA, OCT biomarkers, diagnosis, and medication information (Fig. 1).

Disease	Rules
AMD	<i>'feucht', 'feuchte', 'exsudativ', 'exsudative', *</i> → <i>True</i> <i>'trocken', 'trockene'</i> → <i>False</i>
DME	<i>'diabetisch', 'diabetisches'</i> → <i>True</i> <i>*</i> → <i>False</i>
RVO	<i>'ast', 'retinal', 'zentral'</i> → <i>True</i> <i>*</i> → <i>False</i>

Table 1. Exemplary (German) ophthalmic text processing rules for AMD, DME, and RVO.

2 Methods and implementation

This section provides the methods and their implementation related to the patient progression modelling. Firstly, the proposed system’s architecture for data acquisition, preprocessing, analysis, and prediction is introduced (section 2.1). To allow a unified data processing, the role of the related terminologies for medical application (ophthalmic ontology) is addressed (section 2.2), whereas the data fusion and cleaning is introduced (section 2.3). Subsequently, descriptive statistics are derived (section 2.4). Finally, the principles of the patient progression modelling within the context of our ML- and DL-based approaches are introduced (section 2.5). The related implemented models and approaches to patient progression modelling as well as OCT biomarker classification are provided via open science with the machine learning framework Hexnet³² and can be found on its project page and repository under <https://github.com/TSchlosser13/Hexnet> (see also `_ML/models/contrib`). This study is approved by the *Ethics Committee of the Saxon Medical Association* via the file reference: EK-BR-102/20-2.

2.1 System architecture

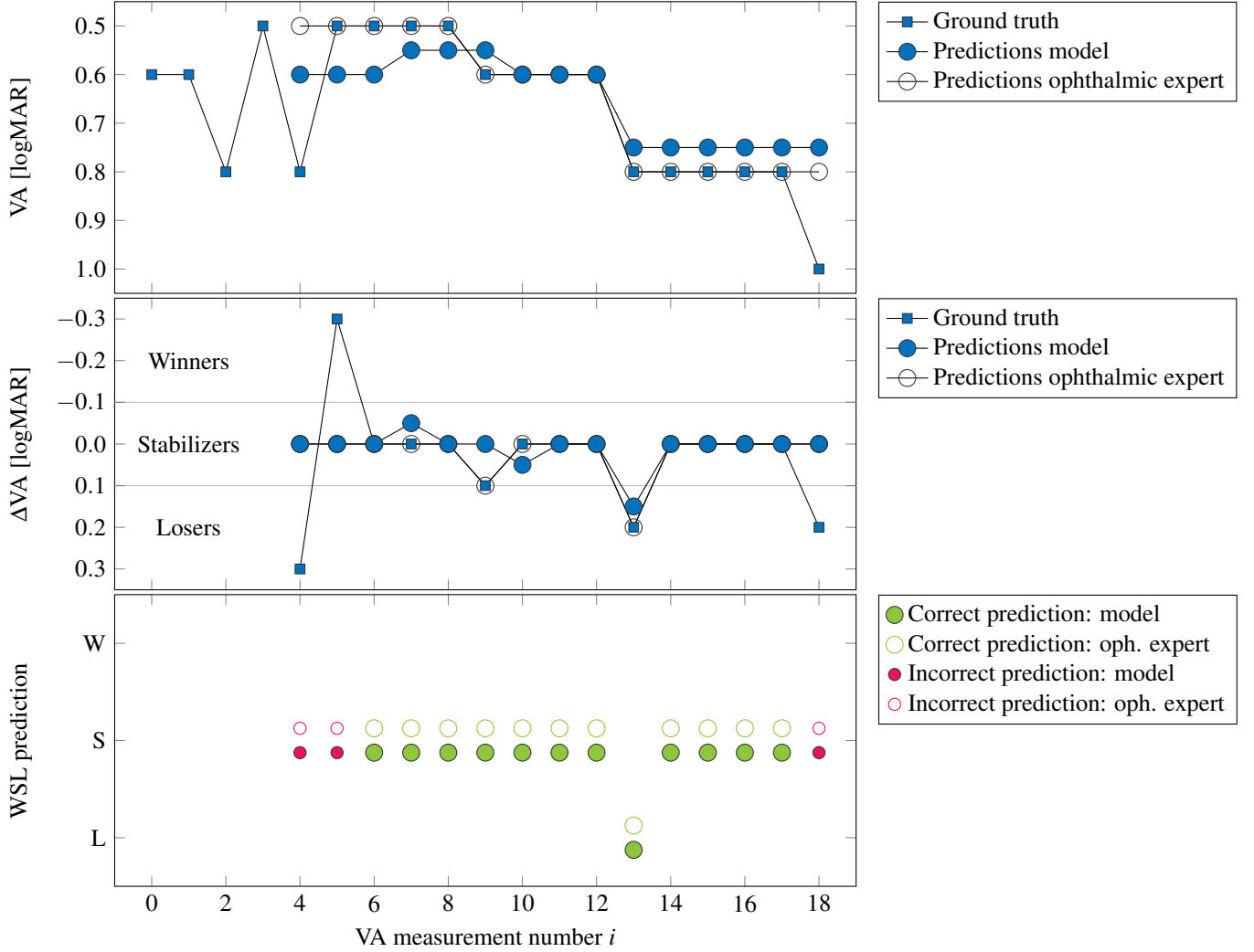
Our ophthalmic core data set obtained from data as well as text mining is based on the categories of general patient information (*G*), VA-based patient information (*V*), OCT scans and biomarkers (*O*), diseases (*D*), as well as treatments and medications (*T*). These categories are obtained from different base systems, the electronic health record system (EHR system, Turbomed), the clinical information system (CIS system, SAP), and an OCT system (Heidelberg Eye Explorer) (see also Fig. 2). While all three systems contain basic patient information, the OCT system provides first and foremost OCT scans (categories *G* and *O*). The EHR system consists of one large database which contains all relevant patient information within the categories of *G*, *V*, *D*, and *T*. As the treatment and medication information within the EHR system is not always complete, the clinic’s CIS system is additionally utilized in order to retrieve missing medication and therapy information (category *CIS*). Following the retrieved data of all three base systems in the form of BDT (EHR system), CSV (CIS system), and E2E files (OCT system), all relevant information are merged in a patient-centered way. This includes a chronological synchronization of all patient information, whereas sensitive patient information has to be furthermore pseudo-anonymized due to patient data privacy and protection laws. These results are then presented via our patient progression visualization and modelling dashboard (Fig. 1).

2.2 Text processing and ontology

The challenge of the ophthalmic text processing is given by the heterogeneity and incompleteness of the underlying data itself, which are in turn documented by many different medical doctors. For text processing and ontology creation, the programming language Python with the Natural Language Toolkit (NLTK)³³ was utilized. Our implementation encompasses a set of category-specific rules handling abbreviations, negations, and synonyms as well as orthography and grammar variants and mistakes. For this purpose, recognized text strings are mapped into a unique ontology via a dictionary-based stemming³⁴. The results have been qualitatively inspected for reliability and plausibility. A thorough quantitative evaluation of our text processing algorithms is still subject to further investigations and will be part of our future research. Therefore, it is beyond the scope of this contribution to further explain the underlying (German) text processing in detail. In the following, we demonstrate some arbitrary strings from the EHR system’s diagnosis with customized (German) abbreviations and how they are mapped to diseases, whereby “*” denotes a placeholder for any string that is not handled otherwise. The mapping is case-insensitive and was specifically adjusted for German doctors (Table 1).

2.3 Data fusion and cleaning

Our practice management software supports database exports via the BDT file format. Here, we extracted electronic health records from over 10 years ranging from 2010 to 2020, including over 49 000 patients and more than 130 000 examinations. Our six main categories (*G*, *V*, *O*, *D*, *T*, and *OP*) currently span a total of more than 30 subcategories. More than 18 000 IVOMs are available from 2013 to 2020 after a fusion of the EHR and CIS systems’ data. All data were linked to the over 12 000 OCT volumes exported from the OCT system via the patient ID (see also Fig. 2, patient-based data merging).



Subsequently, the obtained merged data table is further processed and cleaned. Firstly, it is cleaned by mapping the arbitrary text strings present in the medical letters to diseases. The medical letters contain several terms and abbreviations for specific diseases as different letters stem from several different doctors (see previous section, Table 1). Secondly, unspecific and invalid terms are revised. For example, the entry “eye side” of treatments is only allowed to have the entries “left” or “right”, while invalid entries such as “-” are removed.

2.4 Category-centered data organization and descriptive statistics

After the data cleaning and fusion, the data are focused towards description of (i) anamnesis, (ii) intravitreal operative medications (IVOMs), (iii) diseases, as well as (iv) visual acuity (Fig. 2). The merged main table is changed towards a patient-centered description. The aim is to record the start and the end dates of anamnesis entries (if available), the diseases, and the IVOM therapy cycles for each patient. We designed our tables via two lines per patient since the diseases are to a large degree eye independent, hence we include both eyes as separate lines in the tables. For the medical doctors, the category-centered tables allow an easier filtering, sorting, and a more compact view of the data for a particular medical information.

Finally, all tables are visualized in the statistical-description module that illustrates for example a single data set. In addition, the tables can also be combined to show cross-table-referenced data correlations. From all available visualizations, including up to 30 combinations of visual acuity and disease statistics, we illustrate in this work due to space limitations the statistics of the aforementioned three diseases, and a disease statistic under the influence of a second disease. As statistical tests, we employ two-sample Student’s t-tests. Furthermore, we quantify the strength of the effect – increase or decrease in visual acuity – via the standard Cohen’s d metric³⁵. Cohen’s d measures it in standard units and stands of 0.2 for a small, 0.5 for a medium, and ≥ 0.8 for a large effect size³⁵. It is calculate via Eq. 1.

$$d = \frac{\bar{x}_1 - \bar{x}_2}{s} \quad (1)$$

Where \bar{x}_1 and \bar{x}_2 are the means of the two data sets (patient populations) and s the standard deviation for the data.

2.5 Patient progression modelling

For the OCT biomarker classification and patient progression modelling via VA prediction, a set of prominent as well as conventional approaches from machine learning and deep learning are adapted by utilizing the machine learning library TensorFlow with Keras as its front end. Furthermore, scikit-learn is deployed for all machine learning based models and evaluation procedures. Since extracted medical data from patients’ EHRs originate from ophthalmologists’ documentations, they are defined as our ground truth and serve as training as well as test data.

2.5.1 OCT biomarker classification

In order to complete incomplete OCT biomarker documentations, our multistage system consists of an ensemble of different models for the local (slice-wise) OCT classification, which in turn enables a global (scan-wise) OCT biomarker classification. Within our proposed approach, OCT biomarkers are firstly classified using the provided OCT images of the OCT scans’ slices (OCT B-scans). For the following scan-wise OCT biomarker classification, the slice-wise classifications are combined by utilizing the respectively obtained classification confidences.

Our 6 OCT biomarkers of interest are separated into two states, physiological and pathological, defining two distinct classes. These take the values interrupted (pathological) vs. preserved (physiological) for external limiting membrane (ELM) and ellipsoid zone (ellipsoid) as well as present (pathological) vs. not present (physiological) for foveal depression, scars, pigment epithelial detachment (PED), and subretinal fibrosis, respectively. An OCT biomarker data set overview with the available OCT B-scans per OCT biomarker and related classes is shown in Table 5, resulting in a total of 12 data subsets, for which a classification into pathological vs. physiological OCT scans is conducted. For our OCT biomarker OCT slice extraction, we determined an intermediate subset of slices with a slice range of 8 to 18 from 25 in total. Since different OCT scans may possess different original image resolutions, their image resolution was scaled to an initial size of 256×256 pixels.

Based on the obtained OCT biomarker classifications, the subsequent VA modelling is realized as a time series prediction using, among others, different ML- and DL-based models such as multilayer perceptrons (MLP)³⁶ and recurrent neural networks^{37,38}.

2.5.2 Visual acuity prediction

To allow a WSL-based grouping of VA values, the logMAR score of each VA value is derived via $VA_{logMAR} = -\log_{10} VA_{dec}$ ³⁹. We define a decimal VA range of 0.04 to 2.0, corresponding to a logMAR range of 1.4 to -0.3 . For the local VA ΔVA_i of the examination i , two adjacent VA values are compared via $\Delta VA_i = VA_i - VA_{i-1}$. A threshold of 0.1 logMAR units divides examination i : $\Delta VA_i < -0.1$ into winners, $-0.1 \leq \Delta VA_i \leq 0.1$ into stabilizers, and $\Delta VA_i > 0.1$ into losers (see also Fig. 3).

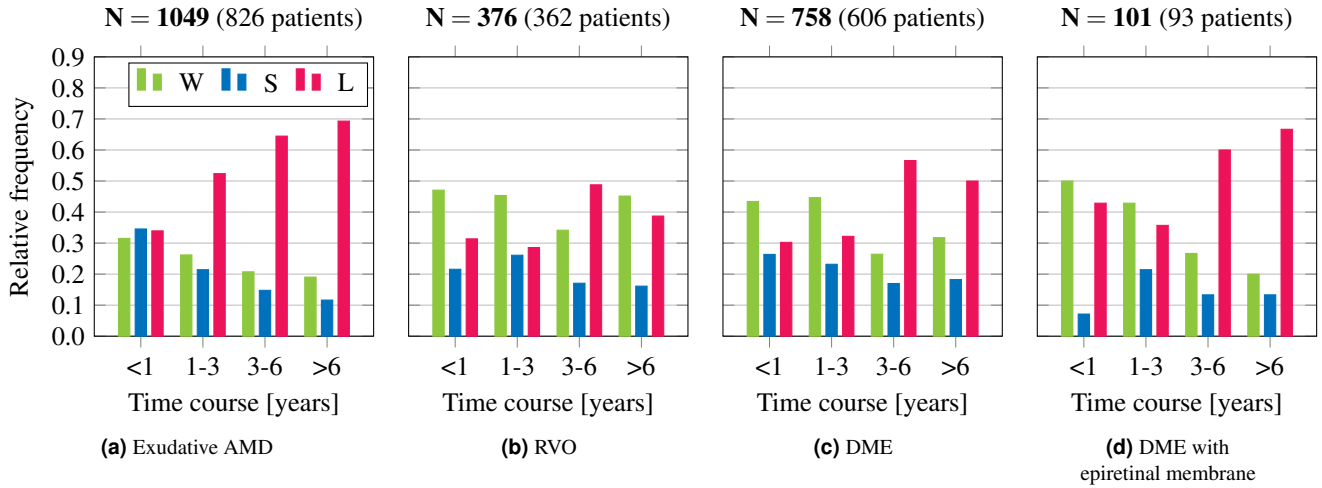


Figure 4. (a–c) Real-world winner, stabilizer, and loser distribution (WSL) for exudative AMD, RVO, and DME. (d) Distribution for the disease DME under exemplary medical co-factor of an epiretinal membrane. The shown results are based on our disease statistics (Fig. 2), whereas N denotes the number of eyes for the given number of patients.

Condition	Significant?	t	p value	Cohen's d
AMD, <1y compared to 1-3y	1	3.09	0.0020	0.30
AMD, <1y compared to >3y	1	6.49	< 0.0001	0.70
RVO, <1y compared to >3y	0	1.89	0.0607	0.38
DME, <1y compared to >3y	1	3.19	0.0016	0.40
DME compared to DME+ERM, >6y	0	1.16	0.2477	0.32

Table 2. Summary of the statistical test results regarding the significant deterioration of the visual acuity. The deterioration is expressed by an increase in the loser fraction. Containing for each tested condition, t-tests were conducted using an alpha parameter of 0.05 (false discovery rate). For example, the first row compares the amount of losers in under 1 year time passed for the disease AMD with the condition of 1-3 years passed. The values refer to the t, p, and Cohen's d value. Cohen's d measures the magnitude of the effect (effect size). A value of 0.2 stands for a small, 0.5 for a medium and ≥ 0.8 for a large effect, whereby medium and large effects are marked in bold.

Table 6 in the appendix gives an overview over our ophthalmic data set with its data organization for VA prediction as it is provided to our predictive models. To predict the VA at a given date, machine learning models typically require a fixed data input size, i.e. a matrix or vector of fixed dimensions. In Table 6, the data organization of an exemplary time window of 4 VA measurements is shown for the first 10 of 24 lines of the feature vector in (a) and for all lines with an example in (c), while (b) explains all 24 medical features associated with each VA's feature vector including "treatment", "OCT biomarker", as well as "additional data". In (c), "–1" denotes the numeric placeholder when no information is present within the respective data fields. Shown are the values for the first window of size 4 in Fig. 1. Our analyses currently include only IVOM therapies and data vectors without therapeutic interventions. In order to make predictions for time windows of different sizes, we define a matrix with predefined dimensions of 24 rows (see, medical feature vector in Table 6 (b)) and 10 columns, which corresponds to 10 time steps or date entries with available information. The minimum time window size is 4, which means that the first 4 of in total 10 columns of the matrix are filled with patient data exemplary shown in Table 6 (b). The remaining 6 columns are set to "–1", especially when no more temporal information is available. The window is – as far as more temporal data are available – iteratively increased by one, i.e., in each iteration, one column more is filled with values and either the subsequent VA is modelled or whether the VA improves, remains constant or worsens (WSL). However, at maximum, 10 time steps (columns) are used given that the visual acuity for the 11th time step is known. Formally, all models in Table 4 require a vector as input. Thus, the matrix was reshaped into a 1×240 vector to be used in model training and testing.

OCT biomarker	Slice-wise F1-score [%]					Scan-wise F1-score [%]
	Logistic Regression ⁴⁰	Random Forest Classifier ⁴⁰	Multilayer Perceptron Classifier ³⁶	DenseNet-201 ⁴¹	ResNet-152V2 ⁴²	Random Forest Classifier ⁴⁰
ELM	85.4 ± 2.1	92.1 ± 1.4	95.3 ± 0.9	96.2 ± 0.6	98.3 ± 0.5	99.9 ± 0.1
Ellipsoid	82.7 ± 1.7	93.8 ± 1.4	96.1 ± 0.7	97.3 ± 1.2	98.7 ± 1.1	99.9 ± 0.1
Foveal depression	56.0 ± 3.4	69.4 ± 0.9	77.3 ± 2.5	75.9 ± 2.3	77.5 ± 2.4	99.9 ± 0.1
Scars	63.8 ± 0.9	72.2 ± 1.0	74.5 ± 1.3	77.2 ± 1.2	77.6 ± 1.0	98.3 ± 1.2
PED	50.4 ± 1.4	63.6 ± 0.9	64.0 ± 1.1	69.0 ± 1.0	67.3 ± 0.9	94.8 ± 0.5
Subretinal fibrosis	69.3 ± 1.5	70.6 ± 0.6	74.5 ± 0.4	75.1 ± 0.2	74.6 ± 0.3	96.2 ± 0.9
Mean	67.9	77.0	80.3	81.8	82.3	98.2

Table 3. OCT biomarker classification results for the slice-wise as well as the scan-wise OCT biomarker classification. We conducted our test runs with a randomized data set split ratio of 80/10/10 for training, validation, and test set averaged over five runs. For our OCT biomarker data set overview, see Table 5.

3 Test results, evaluation, and discussion

The following sections provide our evaluation regarding the predictive statistics of therapy winners, stabilizers, and losers (section 3.1). To allow the inclusion of OCT biomarkers into the patient progression and VA modelling process, incomplete or missing OCT documentations are completed (section 3.2). Given each patient’s medical data, the following patient progression and VA prediction utilizes the resulting OCT biomarker completions (section 3.3).

3.1 Predictive statistics

For the following predictive statistics, a statistical analysis was conducted for our diseases exudative AMD, RVO, and DME. The progression of the VA was classified into therapy winners, stabilizers, and losers (WSL scheme), based on the first and the last VA measurement of each patient (section 2.4). The size of our data corpus and its harmonization as described in sections 2.1 to 2.3 allows different kinds of statistical surveys, e.g. separated according to disease, time periods, and comorbidities. The data originate from a large- and daily-operating medical hospital (German hospital maximum care level) and thus indicate effects of real-world scenarios.

Our statistical investigations consequently allow us to make statistical predictions under real-life conditions for questions such as “If a patient has exudative AMD, what are the future prognoses for this patient?”. For the three aforementioned diseases, the outcomes are shown in Fig. 4. Especially for AMD, in average, a deterioration of the visual acuity over time is observable. A more fine-grained analysis reveals effects over time since we split the data of a disease into patients with short and longer progression. The time course refers to the time difference (in years) between the first and the last VA measurement of individual patients. The total data of $N = 1049$ eyes of AMD is now divided into 4 substatistics with different time windows, whereby, for example, the data in the first time bin of under 1 year is about 25 %. We found, with regard to longer disease time courses, the proportion of losers increases further till > 60 % for time courses of > 6 years and longer. Note that our group WSL definition using ΔVA_{logMAR} thresholds of 0.1 is fixed for all time windows which might be regarded as a somewhat harsh criterion for long time scales. We perform two-sample Student’s t-tests to analyze the statistical significance of the deterioration of the visual acuity, shown in Table 2. To avoid thresholding effects, we perform the tests directly at the raw delta logMAR values. It is found a strong significant effect for the disease AMD ($p < 0.0001$), no significance for RVO ($p = 0.0607$), and a weak significant effect for DME ($p = 0.0016$). A full combination of all statistical tests can be found in the appendix, Table 8. In addition, we employed the Cohen’s d measurement that shows the normalized strength of the effect, i.e. the amount of increase of the loser portion (section 2.4). We observed a deterioration of the visual acuity in AMD with a large/medium effect (Table 2), while the other diseases arouse smaller effects. This means that more and more patients are experiencing deterioration of vision over longer periods of time, especially for AMD.

The representation of our diseases in combination with medical co-factors (comorbidities) is shown in Fig. 4d and can be performed as a proof of concept. It illustrates the influence of an epiretinal membrane (ERM) on the disease DME. Yet, if DME and epiretinal membrane occur simultaneously, it becomes apparent that only about 12–25 patients are included in each substatistic and the direct comparison with the DME-only group would not yet stand up to statistical tests (Table 2). For such substatistics, more data will be needed in the future, e.g., by merging several ophthalmic hospitals into a common research data infrastructure.

Model	Macro average F1-score [%]	
	Feature vectors containing VA values only	Feature vectors containing additional medical data
Model predictions		
Statistical estimator	32.8 ± 0.4	/
MA estimator	29.6 ± 0.3	/
Weighted MA estimator	22.6 ± 0.4	/
Bagging regressor ⁴⁰	40.8 ± 0.2	41.3 ± 0.5
Random forest regressor ⁴⁰	39.9 ± 0.1	40.7 ± 0.4
RNN with LSTM ^{28,37}	37.6 ± 0.3	39.0 ± 0.3
RNN with GRU ^{28,38}	38.1 ± 0.3	39.1 ± 0.1
MLP ³⁶	40.2 ± 0.4	44.6 ± 0.6
MLP-LDA ^{36,40}	44.9 ± 4.5	69.0 ± 5.2
MLP / MLP-LDA w/o annot. OCT biom.	42.9 ± 0.4	63.1 ± 4.7
MLP / MLP-LDA w/o class. OCT biom.	42.7 ± 0.6	62.8 ± 3.1
Annotations		
Ophthalmic expertise	57.8	

Table 4. VA modelling results overview for our approaches with feature vectors containing VA values only / additional medical data (Table 6b) as well as our annotations (ophthalmic expertise) averaged over five runs. “/” denotes model predictions without additional medical data and VA values only. For our VA modelling data set overview with data explanations and vectors, see Table 6. Figures 5 and 6 as well as Table 7 show our evaluation results in further detail.

3.2 OCT biomarker classification

Table 3 shows our classification results for the slice-wise and the scan-wise OCT classification using different prominent approaches from machine learning and deep learning averaged over five runs. In comparison, the selected models DenseNet-201⁴¹ and ResNet-152V2⁴² show the best classification accuracies in F1-score with mean classification accuracies of 81.8 and 82.3 % for our 6 OCT biomarkers. When comparing the results for the different OCT biomarkers, ELM and ellipsoid show the best scan-wise accuracies, whereas subretinal fibrosis and PED represent the more challenging OCT biomarkers. For the following scan-wise OCT classification, a random forest classifier⁴⁰ is already sufficient in order to achieve high classification accuracies of up to 99.9 %. Finally, we obtain the resulting mean classification accuracies in F1-score of 82.3 (slice-wise) and 98.2 % (scan-wise).

3.3 Visual acuity prediction

The principles of VA prediction are illustrated in Fig. 3 for an exemplary patient whose first diagnosis was cataract in both eyes and DME in the right eye in 02/2014. Shown is the VA progression over a timespan of 1 year, in which the patient had 6 IVOMs with Eylea and Lucentis. Our model predicts the $(i + 4)$ th VA value from a time window of the previous four VA measurements up to a size of 10 measurements, e.g., the minimum interval $[i, i + 3]$ with $i = 0, 1, \dots, i_{\max} - 4$. The last documented VA measurement is defined to be i_{\max} . The model uses medical patient with the aforementioned growing window size, which is reformatted as data input matrix as shown in Table 6b. For instance, the 5th VA value will be predicted from patient data of the time interval provided by the 1st to the 4th VA measurement, whereas the 6th VA value will be predicted via the 1st to the 5th measurement. For evaluation, the horizontal lines indicate our thresholds for therapy winners, stabilizers, and losers (see also section 3.1).

3.3.1 Evaluation principles

Out of 49 000 patients, 7 878 patients with VA series of length $i_{\max} \geq 5$ exist within our data, resulting in over 100 000 separate VA series of length 5. With the three diseases AMD, DME, and RVO, 1 496 patients with VA series of length ≥ 5 exist, resulting in 14 026 separate VA series of length 5. For the evaluation, all changes within all consecutive VA-based predictions are considered. Hence, all predictions as shown in Fig. 3 are utilized in order to formulate a prediction capability assessment. The VA-based prediction accuracy is calculated via all VA predictions and related local ΔVA_i . For the modelling process, the completed OCT documentations (section 3.2) and the related additional data is retrieved. For this purpose, Table 6 gives an extensive overview over the leveraged data set as well as the related data organization.

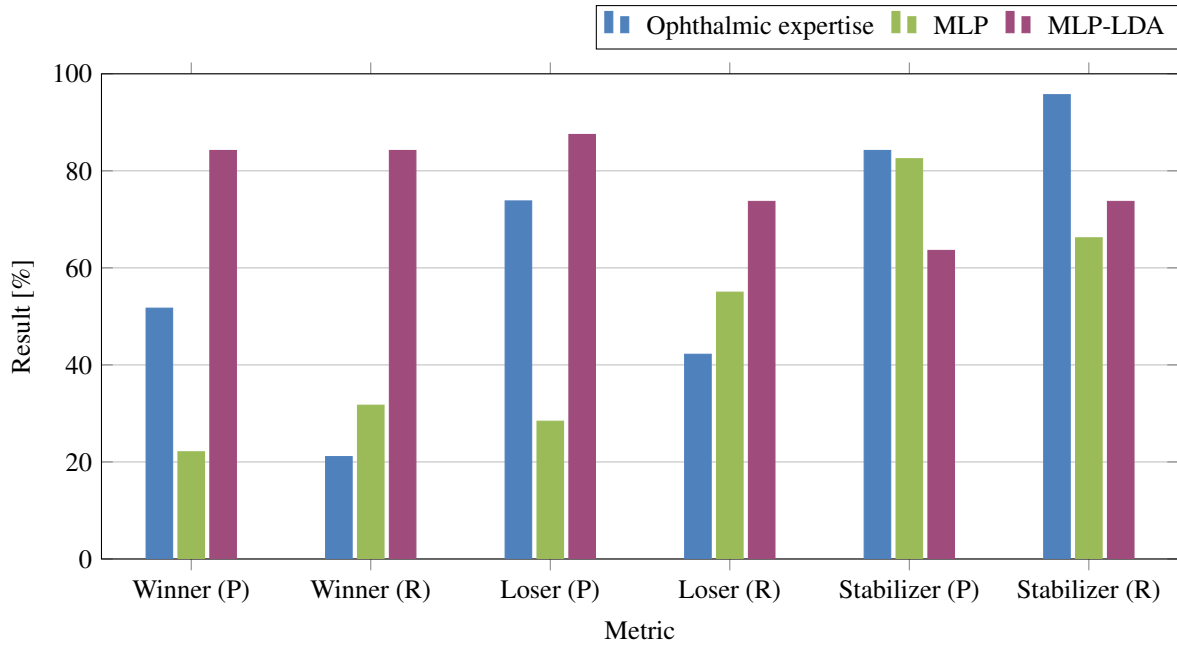


Figure 5. VA modelling results’ precision (P) and recall (R) plot for our annotations (ophthalmic expertise) as well as our approaches to VA prediction with MLP and MLP-LDA based on our WSL scheme (see also Table 7).

3.3.2 Training and test setup

Our training setup for VA prediction includes: the Glorot initializer⁴³ for weight initialization, the Adam optimizer⁴⁴ with a standard learning rate of 0.001 and exponential decay rates of 0.9 and 0.999, as well as a batch size of 32. We conducted our test runs with a randomized data set split ratio of 80/10/10 for training, validation, and test set.

3.3.3 Visual acuity prediction results

Table 4 shows our prediction results using different statistical approaches as well as prominent approaches from machine learning and deep learning averaged over five runs. For this purpose, our statistical estimator predicts VA progressions utilizing the statistical distribution of our WSL scheme within our train set. The moving average (MA) estimator averages the given window of VA values, whereas the weighted MA estimator weights recent VA values more strongly in order to formulate a baseline prediction. Whereas our baseline approaches result in prediction accuracies of up to 40.8 % in macro average F1-score (bagging regressor⁴⁰), a more realistic setting includes the completed OCT documentations with the additional data shown in Table 6. Our MLP-based predictor results in the second highest prediction accuracy, whereas the addition of OCT biomarkers allows their inclusion in the VA modelling process, resulting in a prediction accuracy of 44.6 % with an improvement by 4.4 %. Therefore, the inclusion of OCT biomarkers allows their modelling as crucial information and influential visual factors when no OCT classifications are provided. Following our MLP model, a meta model was realized that classifies the predicted VA values via our WSL scheme. While the MLP predicts the VA values, our so-called MLP-LDA model utilizes these predictions by further classifying them via a linear discriminant analysis (LDA)⁴⁰ into the WSL scheme classes. During the process, the obtained results are cross-validated. We obtain a final prediction accuracy of 69 % (+24.4 %), while the predictions of our ophthalmic expertise reach 57.8 %. Figure 5 gives an overview over our obtained main results in precision and recall for therapy winners, stabilizers, and losers. Considering the class-wise scores, MLP-LDA strikes a balance between all three progression groups, whereas a trade-off between therapy winners and losers with therapy stabilizers is observable. Finally, Table 7 depicts an extensive VA modelling results overview with confusion matrices and class-wise recall and precision results of all VA modelling experiments with MLP, MLP-LDA, and the human reference annotation results from our ophthalmic expertise. In comparison to MLP and MLP-LDA, our annotations show increased scores for therapy stabilizers while achieving the highest total in true positives. However, MLP-LDA achieves a by 11.2 % increased macro average F1-score (69 vs. 57.8 %, Table 4) while showing only a by 5 % reduced accuracy in true positives (77.2 vs. 82.2 %, Table 7). We conclude that treatment winners and losers are predicted with increased accuracy by our best model compared to our ophthalmic expertise in both recall and precision, which is a promising result. However, as treatment stabilizers, which are in turn predominantly present in our data corpus, are predicted worse, an improvement of the VA prediction for stabilizers has to be enforced to realize a

(semi-)automated recommender system. Finally, in order to further validate the annotations of our ophthalmic expertise, we evaluated the annotations of seven different additional ophthalmic doctors given randomized subsets of our data set, obtaining a combined prediction accuracy in macro average F1-score of 50.0 ± 10.7 % (37.7–69.4 % with a range of 31.7 %).

4 Conclusion and outlook

In this contribution, we developed an IT system architecture that aggregates patient-wise information for more than 49 000 patients from different categories of various multimedia data in the form of text and images within multiple heterogeneous ophthalmic data resources originating from a German hospital of maximum care. As the prediction of a patient's progression is challenging within this real-world setting, our realized workflow allows a first processing of medical patient data to enable a visual acuity prediction, OCT biomarker classification, as well as a general statistical evaluation and visualization.

The resulting data corpus allows predictive statements of the expected progression of a patient and his or her visual acuity in each of the three diseases of AMD, DME, and RVO. Our data reveal that especially exudative AMD results in a notable high amount of therapy “losers” (56 % regarding a time span of 3 to 6 years). The result for AMD is significant. Furthermore, we found a weak-significant deterioration of visual acuity for DME, while no significant deterioration for RVO. A more fine-grained analysis is able to reveal the influence of medical co-existing factors such as other diseases. As proof of concept, we exemplary show DME with an epiretinal membrane. Yet, the data situation is still too weak to derive reliable correlations for statistical surveys of comorbidities in combination with different observation time windows.

For the following visual acuity based treatment progression modelling, incomplete OCT documentations are completed by classifying the OCT scans' slices (OCT B-scans), which in turn allows the classification of OCT scans when only single OCT slices are provided. Based on the obtained OCT slice classifications, a scan-wise OCT classification of the OCT biomarkers ELM, ellipsoid zone, foveal depression, scars, PED, and subretinal fibrosis resulted in an overall classification accuracy (F1-score) of over 98 %. Finally, the completed OCT documentations are combined with additional medical data, defining our ophthalmic feature vectors for visual acuity prediction. In comparison to different approaches from machine learning and deep learning, we achieve an overall prediction accuracy of up to 69 % (macro average F1-score), whereas our ophthalmic expertise reaches an overall prediction performance of 57.8 % (+11.2 %).

However, as the influence of the OCT biomarkers is not yet fully understood, further investigations have to be conducted, for which additional OCT biomarkers as well as their influence for the visual acuity modelling process have to be evaluated. Future contributions can build on these initial results in order to determine an optimal time for a change in medication or therapy. This also encompasses treatment options such as laser coagulation, pars plana vitrectomy, or phacoemulsification with posterior chamber lens implantation. We aim to extend our approach to include a larger data corpus through distributed analysis across multiple ophthalmic sites. The quality of the data needs to be ensured via comprehensive evaluations of our medical texts structured by rule- and learning based NLP methods, which requires further harmonization of the underlying medical terminology. Patient-related data of the different categories available and their relevance for the modelling process have to be further investigated in order to increase the evidence of AI-based modelling approaches to enable future realizations of a (semi-)automated recommender system.

Acknowledgment

This research was partially funded by the European Social Fund for Germany, the Novartis Pharma GmbH, as well as the Federal Ministry of Education and Research, namely the *Medical Informatics Hub in Saxony (MiHUBx)* with the grant numbers 01ZZ2101E (Klinikum Chemnitz) and 01ZZ2101C (Chemnitz University of Technology).

Author contributions

Tobias Schlosser, Frederik Beuth, Trixy Meyer, and Danny Kowerko conducted this contribution's writing process and the related research project's implementation and evaluation with the help of Arunodhayan Sampath Kumar, Gabriel Stolze, Olga Furashova, and Katrin Engelmann in revising this manuscript, whereas Olga Furashova, Katrin Engelmann, and Danny Kowerko designed and supervised the related research project.

Additional Information

The authors declare that they have no conflict of interest.

Data Availability

Not applicable

References

1. Nimse, S. B., Sonawane, M. D., Song, K.-S. & Kim, T. Biomarker detection technologies and future directions. *Analyst* **141**, 740–755, DOI: [10.1039/C5AN01790D](https://doi.org/10.1039/C5AN01790D) (2016).
2. Seeböck, P. *et al.* Exploiting Epistemic Uncertainty of Anatomy Segmentation for Anomaly Detection in Retinal OCT. *IEEE Transactions on Med. Imaging* **39**, 87–98, DOI: [10.1109/TMI.2019.2919951](https://doi.org/10.1109/TMI.2019.2919951) (2019).
3. Finger, R. P., Wiedemann, P., Blumhagen, F., Pohl, K. & Holz, F. G. Treatment patterns, visual acuity and quality-of-life outcomes of the WAVE study – A noninterventonal study of ranibizumab treatment for neovascular age-related macular degeneration in Germany. *Acta Ophthalmol.* **91**, 540–546, DOI: [10.1111/j.1755-3768.2012.02493.x](https://doi.org/10.1111/j.1755-3768.2012.02493.x) (2012).
4. Hykin, P. *et al.* A retrospective study of the real-life utilization and effectiveness of ranibizumab therapy for neovascular age-related macular degeneration in the UK. *Clin. Ophthalmol.* **10**, 87–96, DOI: [10.2147/OPTH.S92627](https://doi.org/10.2147/OPTH.S92627) (2016).
5. Wintergerst, M. W. M. *et al.* Pro-re-nata-anti-VEGF-Behandlungsergebnisse bei neovaskulärer altersabhängiger Makuladegeneration in der klinischen Routineversorgung: Vergleich von Einzel- mit 3er-Injektionen. *Der Ophthalmol.* **116**, 441–446, DOI: [10.1007/s00347-018-0747-4](https://doi.org/10.1007/s00347-018-0747-4) (2019).
6. Gerding, H., Loukopoulos, V., Riese, J., Hefner, L. & Timmermann, M. Results of flexible ranibizumab treatment in age-related macular degeneration and search for parameters with impact on outcome. *Graefe's Arch. for Clin. Exp. Ophthalmol.* **249**, 653–662, DOI: [10.1007/s00417-011-1636-6](https://doi.org/10.1007/s00417-011-1636-6) (2011).
7. Gerendas, B. S., Waldstein, S. M. & Schmidt-Erfurth, U. Screening und Management retinaler Erkrankungen mittels digitaler Medizin. *Der Ophthalmol.* **115**, 728–736, DOI: [10.1007/s00347-018-0752-7](https://doi.org/10.1007/s00347-018-0752-7) (2018).
8. Schmidt-Erfurth, U. *et al.* Role of Deep Learning–Quantified Hyperreflective Foci for the Prediction of Geographic Atrophy Progression. *Am. J. Ophthalmol.* **216**, 257–270, DOI: [10.1016/j.ajo.2020.03.042](https://doi.org/10.1016/j.ajo.2020.03.042) (2020).
9. Waldstein, S. M. *et al.* Characterization of Drusen and Hyperreflective Foci as Biomarkers for Disease Progression in Age-Related Macular Degeneration Using Artificial Intelligence in Optical Coherence Tomography. *JAMA Ophthalmol.* **138**, 740–747, DOI: [10.1001/jamaophthalmol.2020.1376](https://doi.org/10.1001/jamaophthalmol.2020.1376) (2020).
10. Spaide, R. F. *et al.* Consensus Nomenclature for Reporting Neovascular Age-Related Macular Degeneration Data. *Ophthalmology* **127**, 616–636, DOI: [10.1016/J.OPHTHA.2019.11.004](https://doi.org/10.1016/J.OPHTHA.2019.11.004) (2020).
11. Matsui, Y. *et al.* Which Explanatory Variables Contribute to the Classification of Good Visual Acuity over Time in Patients with Branch Retinal Vein Occlusion with Macular Edema Using Machine Learning? *J. Clin. Medicine* **11**, 3903, DOI: [10.3390/JCM11133903](https://doi.org/10.3390/JCM11133903) (2022).
12. Chen, Y. M., Huang, W. T., Ho, W. H. & Tsai, J. T. Classification of age-related macular degeneration using convolutional-neural-network-based transfer learning. *BMC Bioinforma.* **22**, 1–16, DOI: [10.1186/S12859-021-04001-1/FIGURES/6](https://doi.org/10.1186/S12859-021-04001-1/FIGURES/6) (2021).
13. Phan, L. T., Broadhead, G. K., Hong, T. H. & Chang, A. A. Predictors of Visual Acuity After Treatment of Neovascular Age-Related Macular Degeneration – Current Perspectives. *Clin. Ophthalmol.* **15**, 3351–3367, DOI: [10.2147/OPTH.S205147](https://doi.org/10.2147/OPTH.S205147) (2021).
14. Romond, K. *et al.* Imaging and artificial intelligence for progression of age-related macular degeneration. *Exp. Biol. Medicine* **246**, 2159–2169, DOI: [10.1177/15353702211031547](https://doi.org/10.1177/15353702211031547) (2021).
15. Porwal, P. *et al.* Indian Diabetic Retinopathy Image Dataset (IDRiD): A Database for Diabetic Retinopathy Screening Research. *Data* **3**, DOI: [10.3390/data3030025](https://doi.org/10.3390/data3030025) (2018).
16. Pachade, S. *et al.* Retinal Fundus Multi-Disease Image Dataset (RFMiD): A Dataset for Multi-Disease Detection Research. *Data* **6**, DOI: [10.3390/data6020014](https://doi.org/10.3390/data6020014) (2021).
17. Khanani, A. M. *et al.* SIERRA-AMD: A Retrospective, Real-World Evidence Study of Patients with Neovascular Age-Related Macular Degeneration in the United States. *Ophthalmol. Retin.* **4**, 122–133, DOI: [10.1016/j.oret.2019.09.009](https://doi.org/10.1016/j.oret.2019.09.009) (2020).
18. Rößner, M., Kahl, S., Engelmann, K. & Kowerko, D. Preparing clinical ophthalmic data for research application. In *INFORMATIK 2017*, 2231–2240, DOI: [10.18420/in2017{_}222](https://doi.org/10.18420/in2017{_}222) (2017).
19. Xu, H. *et al.* MedEx: a medication information extraction system for clinical narratives. *J. Am. Med. Informatics Assoc.* **17**, 19–24, DOI: [10.1197/jamia.M3378](https://doi.org/10.1197/jamia.M3378) (2010).
20. Wang, S. Y., Pershing, S., Tran, E. & Hernandez-Boussard, T. Automated extraction of ophthalmic surgery outcomes from the electronic health record. *Int. J. Med. Informatics* **133**, DOI: [10.1016/j.ijmedinf.2019.104007](https://doi.org/10.1016/j.ijmedinf.2019.104007) (2020).

21. Wang, S. Y., Tseng, B. & Hernandez-Boussard, T. Development and evaluation of novel ophthalmology domain-specific neural word embeddings to predict visual prognosis. *Int. J. Med. Informatics* **150**, DOI: [10.1016/j.ijmedinf.2021.104464](https://doi.org/10.1016/j.ijmedinf.2021.104464) (2021).
22. Hu, W. & Wang, S. Y. Predicting Glaucoma Progression Requiring Surgery Using Clinical Free-Text Notes and Transfer Learning With Transformers. *Transl. Vis. Sci. & Technol.* **11**, DOI: [10.1167/tvst.11.3.37](https://doi.org/10.1167/tvst.11.3.37) (2022).
23. Fauw, J. D. *et al.* Clinically applicable deep learning for diagnosis and referral in retinal disease. *Nat. Medicine* **24**, 1342–1350, DOI: [10.1038/s41591-018-0107-6](https://doi.org/10.1038/s41591-018-0107-6) (2018).
24. Kurmann, T. *et al.* Expert-level Automated Biomarker Identification in Optical Coherence Tomography Scans. *Sci. Reports* **9**, 1–9, DOI: [10.1038/s41598-019-49740-7](https://doi.org/10.1038/s41598-019-49740-7) (2019).
25. Zadeh, S. G. *et al.* CNNs Enable Accurate and Fast Segmentation of Drusen in Optical Coherence Tomography. In *International Workshop on Multimodal Learning for Clinical Decision Support (ML-CDS 2017)*, 65–73, DOI: [10.1007/978-3-319-67558-9_8](https://doi.org/10.1007/978-3-319-67558-9_8) (2017).
26. Terheyden, J. H. *et al.* Automated thresholding algorithms outperform manual thresholding in macular optical coherence tomography angiography image analysis. *PLOS ONE* **15**, DOI: [10.1371/journal.pone.0230260](https://doi.org/10.1371/journal.pone.0230260) (2020).
27. Schlegl, T. *et al.* Fully Automated Segmentation of Hyperreflective Foci in Optical Coherence Tomography Images (2018). DOI: [10.48550/arXiv.1805.03278](https://doi.org/10.48550/arXiv.1805.03278).
28. Rumelhart, D. E., Hinton, G. E. & Williams, R. J. Learning representations by back-propagating errors. *Nature* **323**, 533–536, DOI: doi.org/10.1038/323533a0 (1986).
29. Wang, T., Qiu, R. G. & Yu, M. Predictive Modeling of the Progression of Alzheimer’s Disease with Recurrent Neural Networks. *Sci. Reports* **8**, 1–12, DOI: [10.1038/s41598-018-27337-w](https://doi.org/10.1038/s41598-018-27337-w) (2018).
30. Edwards, D. A. *et al.* Mathematical models for the effect of anti-vascular endothelial growth factor on visual acuity. *J. Math. Biol.* **81**, 1397–1428, DOI: [10.1007/s00285-020-01544-4](https://doi.org/10.1007/s00285-020-01544-4) (2020).
31. DaCosta, J., Bhatia, D. & Talks, J. The use of optical coherence tomography angiography and optical coherence tomography to predict visual acuity in diabetic retinopathy. *Eye* **34**, 942–947, DOI: [10.1038/s41433-019-0606-9](https://doi.org/10.1038/s41433-019-0606-9) (2020).
32. Schlosser, T., Friedrich, M., Meyer, T., Kowerko, D. & Eibl, M. Biologically Inspired Hexagonal Deep Learning for Hexagonal Image Processing With The Hexagonal Image Processing Framework Hexnet. *IEEE Transactions on Image Process. (Preprint)* (2022).
33. Bird, S., Klein, E. & Loper, E. *Natural Language Processing with Python: Analyzing Text with the Natural Language Toolkit* (O’Reilly Media, 2009).
34. Porter, M. F. An algorithm for suffix stripping. *Program: electronic library information systems* **14**, 130–137, DOI: [10.1108/eb046814](https://doi.org/10.1108/eb046814) (1980).
35. Cohen, J. *Statistical power analysis for the behavioral sciences* (Taylor & Francis, 1988).
36. Hinton, G. E. Connectionist learning procedures. In *Machine Learning: An Artificial Intelligence Approach, Volume III*, 555–610, DOI: [10.1016/B978-0-08-051055-2.50029-8](https://doi.org/10.1016/B978-0-08-051055-2.50029-8) (Elsevier, 1990).
37. Hochreiter, S. & Schmidhuber, J. Long Short-Term Memory. *Neural Comput.* **9**, 1735–1780, DOI: [10.1162/neco.1997.9.8.1735](https://doi.org/10.1162/neco.1997.9.8.1735) (1997).
38. Chung, J., Gulcehre, C., Cho, K. & Bengio, Y. Empirical Evaluation of Gated Recurrent Neural Networks on Sequence Modeling. In *NIPS 2014 Workshop on Deep Learning*, DOI: [10.48550/arXiv.1412.3555](https://doi.org/10.48550/arXiv.1412.3555) (2014).
39. Schulze-Bonsel, K., Feltgen, N., Burau, H., Hansen, L. & Bach, M. Visual Acuities “Hand Motion” and “Counting Fingers” Can Be Quantified with the Freiburg Visual Acuity Test. *Investig. Ophthalmol. & Vis. Sci.* **47**, 1236–1240, DOI: [10.1167/iovs.05-0981](https://doi.org/10.1167/iovs.05-0981) (2006).
40. Hastie, T., Tibshirani, R. & Friedman, J. *The Elements of Statistical Learning: Data Mining, Inference, and Prediction*, vol. 2 (Springer, 2009).
41. Huang, G., Liu, Z., Maaten, L. V. D. & Weinberger, K. Q. Densely Connected Convolutional Networks. In *2017 IEEE Conference on Computer Vision and Pattern Recognition (CVPR)*, 4700–4708, DOI: [10.1109/CVPR.2017.243](https://doi.org/10.1109/CVPR.2017.243) (2017).
42. He, K., Zhang, X., Ren, S. & Sun, J. Deep Residual Learning for Image Recognition. In *2016 IEEE Conference on Computer Vision and Pattern Recognition (CVPR)*, 770–778, DOI: [10.1109/CVPR.2016.90](https://doi.org/10.1109/CVPR.2016.90) (2016).
43. Glorot, X. & Bengio, Y. Understanding the difficulty of training deep feedforward neural networks. In *Proceedings of the Thirteenth International Conference on Artificial Intelligence and Statistics*, 249–256 (2010).

44. Kingma, D. P. & Ba, J. Adam: A Method for Stochastic Optimization. In *3rd International Conference on Learning Representations (ICLR 2015)*, DOI: [10.48550/arXiv.1412.698](https://doi.org/10.48550/arXiv.1412.6980) (2015).

5 Appendix

5.1 Classification definitions and terminology

The macro average F1-score is calculated via the class-wise F1-scores f , where F denotes the set of all class-wise F1-scores following our WSL scheme: $\text{macro average F1-score} = 1/|F| \cdot \sum_{f \in F} f$, whereas the class-wise F1-scores are in turn calculated via $F1\text{-score} = 2 \cdot (\text{precision} \cdot \text{recall}) / (\text{precision} + \text{recall})$ with $\text{precision} = TP / (TP + FP)$ and $\text{recall} = TP / (TP + FN)$ (TP = classification true positives, FP = false positives, and FN = false negatives).

OCT biomarker	Class		Ratio [phys./path.]
	Physiological	Pathological	
ELM	7660	407	18.8
Ellipsoid	7377	308	24.0
Foveal depression	40087	10923	3.7
Scars	9088	4687	1.9
PED	7866	10635	0.7
Subretinal fibrosis	8481	5261	1.6

Table 5. Ophthalmic data set overview for our 6 different OCT biomarkers. Shown are the available OCT slices per OCT biomarker with their related classes of physiological as well as pathological image samples.

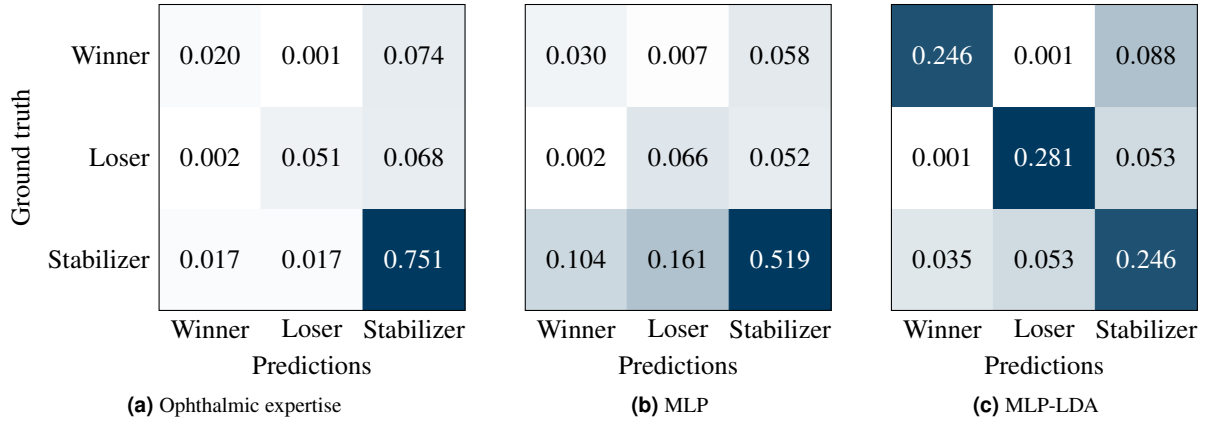


Figure 6. VA modelling results' globally normalized confusion matrices for our annotations (ophthalmic expertise) as well as our approaches to VA prediction with MLP and MLP-LDA based on our WSL scheme.

1	date_ _{j} ,	date_ _{j+1} ,	date_ _{j+2} ,	..., date_ _{i}
2	age_ _{j} ,	age_ _{j+1} ,	age_ _{j+2} ,	..., age_ _{i}
3	VA_ _{j} ,	VA_ _{j+1} ,	VA_ _{j+2} ,	..., VA_ _{i}
4	treatment_ _{j} ,	treatment_ _{j+1} ,	treatment_ _{j+2} ,	..., treatment_ _{i}
5	OCT biomarker_ _{j,1} ,	OCT biomarker_ _{j+1,1} ,	OCT biomarker_ _{j+2,1} ,	..., OCT biomarker_ _{i,1}
6	OCT biomarker_ _{j,2} ,	OCT biomarker_ _{j+1,2} ,	OCT biomarker_ _{j+2,2} ,	..., OCT biomarker_ _{i,2}
7	OCT biomarker_ _{j,3} ,	OCT biomarker_ _{j+1,3} ,	OCT biomarker_ _{j+2,3} ,	..., OCT biomarker_ _{i,3}
8	...,	...,	...,	...
9	OCT biomarker_ _{j,n} ,	OCT biomarker_ _{j+1,n} ,	OCT biomarker_ _{j+2,n} ,	..., OCT biomarker_ _{i,n}
10	additional data_ _{j} ,	additional data_ _{j+1} ,	additional data_ _{j+2} ,	..., additional data_ _{i}

(a) Data organization

Entry	Explanation
1.	Current date in days since the patient's birth
2.	The patient's year of birth
3.	The patient's sex
4.	VA (l/r)
Treatments	
5.	Medication (l/r): Eylea or Lucentis
6.–8.	Related information: apoplexy, blood thinning, and myocardial infarction
OCT scans	
9.–14.	OCT biomarkers (l/r): ELM, ellipsoid, foveal depression, scars, PED, and subretinal fibrosis
15.–17.	Related information (l/r): central retinal thickness as well as intraretinal and subretinal fluid
Additional data	
18.–24.	Diseases (l/r): AMD, DME, and RVV as well as cataract, diabetic retinopathy, ERM, and pseudophakia

(b) Data explanations

1	20177, 20239, 20396, 20519
2	1965, 1965, 1965, 1965
3	0, 0, 0, 0
4	0.8, 0.5, 0.5, 0.5
5	-1, 0, -1, -1
6	-1, -1, -1, -1
7	-1, -1, -1, -1
8	-1, -1, -1, -1
9	-1, -1, -1, -1
10	-1, -1, -1, -1
11	1, 0, -1, -1
12	-1, -1, -1, -1
13	-1, -1, -1, -1
14	-1, -1, -1, -1
15	306, 437, -1, -1
16	-1, -1, 1, -1
17	-1, -1, -1, -1
18	-1, -1, -1, -1
19	1, 0, -1, -1
20	0, 2, -1, -1
21	-1, -1, -1, -1
22	-1, -1, -1, -1
23	-1, -1, -1, -1
24	-1, -1, -1, -1

(c) Data vectors

Table 6. Ophthalmic data set overview with utilized data organization for VA prediction. To predict the VA at date i , a window of maximum window size 10 ($i - j$) is utilized (a). For this purpose, the shown data organization from lines 1 to 10 is deployed, whereas the data within the fields “treatment”, “OCT biomarker”, as well as “additional data” is further detailed in (b). Here, “l/r” denotes the availability of data for both eyes. When translating the information from (a) and (b), factorized data vectors are obtained (c) which are in turn applied to the model learning and evaluation procedures. In (c), “-1” denotes a numeric placeholder when no information is present within the respective data fields. For the sake of simplicity, the processing step of data factorization was omitted. For example, the data entry of the patient's sex can result in three different values: 0 for male, 1 for female, and 2 for patients of diverse sex. Shown are the values for the first window of size 4 in Fig. 1.

Ophthalmic expertise

		Predictions						
		Winner	Loser	Stabilizer	Total	Pro rata [%]	Precision	Recall
Ground truth	Winner	30	2	110	142	9.5	51.7	21.1
	Loser	3	76	101	180	12.1	73.8	42.2
	Stabilizer	25	25	1122	1172	78.5	84.2	95.7
	True positives	1 228 (82.2 %)			1494	Mean	66.3	54.2
					Macro average F1-score			
					57.8			

MLP

Predictions							
	Winner	Loser	Stabilizer	Total	Pro rata [%]	Precision	
Ground truth	Winner	45	10	87	142	9.5	22.1
	Loser	3	99	78	180	12.1	28.4
	Stabilizer	156	240	776	1172	78.5	82.5
True positives	920 (61.6 %)			1494	Mean	45.8	46.7
					Macro average F1-score		45.6

MLP-LDA

		Predictions							
		Winner	Loser	Stabilizer	Total	Pro rata [%]	Precision	Recall	
Ground truth	Winner	70	0	25	95	33.3	84.2	84.2	
	Loser	0	80	15	95	33.3	87.5	73.7	
	Stabilizer	10	15	70	95	33.3	63.6	73.7	
	True positives				220 (77.2 %)	285	Mean	78.4	77.2
					Macro average F1-score				77.5

Table 7. VA modelling results overview for our baseline approaches without additional data (VA values only), ML- and DL-based approaches with additional data, as well as annotations (ophthalmic expertise) of one single run.

5.2 Predictive statistics: complete test results of the statistical tests

Condition	Significant?	t	p value	Cohen's d
AMD, <1y compared to 1-3y	1	3.09	0.0020	0.30
AMD, 1-3y compared to 3-6y	1	4.51	< 0.0001	0.35
AMD, 3-6y compared to >6y	0	0.59	0.5562	0.05
AMD, <1y compared to >3y	1	6.49	< 0.0001	0.70
RVO, <1y compared to 1-3y	0	0.57	0.5692	0.07
RVO, 1-3y compared to 3-6y	1	2.56	0.0110	0.34
RVO, 3-6y compared to >6y	0	0.52	0.6048	0.11
RVO, <1y compared to >3y	0	1.89	0.0607	0.38
DME, <1y compared to 1-3y	0	0.45	0.6500	0.05
DME, 1-3y compared to 3-6y	1	4.98	< 0.0001	0.45
DME, 3-6y compared to >6y	0	0.79	0.4277	0.09
DME, <1y compared to >3y	1	3.19	0.0016	0.40
DME compared to DME+ERM, <1y	0	0.54	0.5860	0.15
DME compared to DME+ERM, 1-3y	0	0.36	0.7178	0.06
DME compared to DME+ERM, 3-6y	0	0.12	0.9002	0.02
DME compared to DME+ERM, >6y	0	1.16	0.2477	0.32

Table 8. Full statistical test results. See Table 2 for details.